

Laser-Induced Inelastic Diffraction from Strong-Field Double Ionization

Wei Quan,¹ XiaoLei Hao,² XiaoQing Hu,³ RenPing Sun,^{1,8} YanLan Wang,^{1,8} YongJu Chen,^{1,8}
ShaoGang Yu,^{1,8} SongPo Xu,^{1,8} ZhiLei Xiao,^{1,8} XuanYang Lai,¹ XingYu Li,³ Wilhelm Becker,^{4,5}
Yong Wu,^{3,*} JianGuo Wang,³ XiaoJun Liu,^{1,†} and Jing Chen^{3,6,7,‡}

¹State Key Laboratory of Magnetic Resonance and Atomic and Molecular Physics and Center for Cold Atom Physics,
Wuhan Institute of Physics and Mathematics, Chinese Academy of Sciences, Wuhan 430071, China

²Institute of Theoretical Physics and Department of Physics, State Key Laboratory of Quantum Optics and Quantum Optics Devices,
Collaborative Innovation Center of Extreme Optics, Shanxi University, Taiyuan 030006, China

³Institute of Applied Physics and Computational Mathematics, P.O. Box 8009, Beijing 100088, China

⁴Max-Born-Institut, Max-Born-Strasse 2a, 12489 Berlin, Germany

⁵Moscow Research Nuclear University MEPhI, 115409 Moscow, Russia

⁶HEDPS, Center for Applied Physics and Technology, Peking University, Beijing 100084, China

⁷Collaborative Innovation Center of IFSA CICI/SA Shanghai Jiao Tong University, Shanghai 200240, China

⁸School of Physics, University of Chinese Academy of Sciences, Beijing 100080, China

(Received 26 July 2017; published 13 December 2017)

In this Letter, we propose a novel laser-induced inelastic diffraction (LIID) scheme based on the intense-field-driven atomic nonsequential double ionization (NSDI) process and demonstrate that, with this LIID approach, the doubly differential cross sections (DDCSs) of the target ions, e.g., Ar⁺ and Xe⁺, can be accurately extracted from the two-dimensional photoelectron momentum distributions in the NSDI process of the corresponding atoms. The extracted DDCSs exhibit a strong dependence on both the target and the laser intensity, in good agreement with calculated DDCSs from the scattering of free electrons. The LIID scheme may be extended to molecular systems and provides a promising approach for imaging of the gas-phase molecular dynamics induced by a strong laser field with unprecedented spatial and temporal resolution.

DOI: 10.1103/PhysRevLett.119.243203

X-ray diffraction and electron diffraction are the conventional methods to determine the structure of molecules and solids with subangstrom spatial resolution. Recent developments have shown that x-ray diffraction using an x-ray pulse with a few-femtosecond duration is capable of taking snapshots of the structural change of a complex molecule during a chemical reaction [1]. However, such photon-based approaches suffer from the coarse spatial resolution and low scattering cross sections, especially for gas-phase targets. In contrast, conventional electron diffraction may provide a much larger scattering cross section and smaller de Broglie wavelength. The challenge for such conventional electron-based approaches is, however, the temporal resolution, which is limited to about several tens of femtoseconds owing to space-charge broadening [2–4].

Over the past decade, we have also witnessed the emergence and rapid development of an alternative imaging approach, which is a self-imaging method based on coherent electron bursts liberated by an intense laser field in the same molecule that they are going to image. The principle underlying this self-imaging approach is the strong-field rescattering model [5,6]. Within this model, an atom or a molecule is first ionized by an intense laser field at some time t_b and an electronic wave packet is started in the continuum. For suitable times t_b , the electron accelerated by the laser field may return to its parent core at

a later time t_r and recollide. During the propagation, the electron may acquire significant kinetic energy from the field. In the recollision at the time t_r , the electron can either recombine or elastically scatter. Based on the former process, high-harmonic-generation (HHG) spectroscopy has been developed to retrieve the atomic structure or to trace in real time the atomic motion during a chemical reaction [7,8]. With the latter, a laser-induced electron-diffraction (LIED) approach has been recently established and extensively employed, e.g., in extracting the angle-dependent electron scattering cross section [9–11]. Moreover, when the de Broglie wavelength of the recolliding electronic wave packet becomes comparable with the molecular dimension, interatomic distances in a molecule can be determined with subangstrom precision and an exposure time of a few femtoseconds [12–14].

Alternatively, at the time t_r , the wave packet may also inelastically scatter off the parent ion, with a second electron being kicked out. This process, termed nonsequential double ionization (NSDI) [15], corresponds exactly to a conventional inelastic collision, i.e., the (e , $2e$) process. In this Letter, we propose a laser-induced inelastic diffraction (LIID) scheme based on this NSDI process. We further demonstrate experimentally that, with this LIID approach, the inelastic scattering cross section of the target ion for free electrons can be accurately extracted

from the photoelectron momentum spectra emitted in the laser-induced (e , $2e$) process. Our conclusion is based on the comparison of the doubly differential cross section (DDCS) extracted from the data with calculations in the context of the distorted-wave Born approximation (DWBA). While our conclusion is derived for atomic targets, LIID can be applied to molecular targets as well. In the molecular case, our procedure may be implemented for ultrafast imaging of transient molecules. Compared to the well-established LIED approach, LIID is expected to obtain more information about the targets during the collision, e.g., the dynamical electron correlation.

Figure 1 presents a graphic sketch of the principle of the LIID procedure. According to the rescattering picture of NSDI [5], for the (e , $2e$) process with one electron released with kinetic energy close to zero, the measured momentum of the other electron can be expressed as

$$\mathbf{p} = \mathbf{p}_z + \mathbf{p}_r, \quad (1)$$

where $\mathbf{p}_z = -\hat{\mathbf{z}}A(t_r)$ denotes the momentum acquired by the electron after the recollision [$A(t)$ is the vector potential of the laser field], and \mathbf{p}_r denotes the residual vector momentum of the electron after the recollision scattered in an arbitrary direction. The maximal final momentum of the

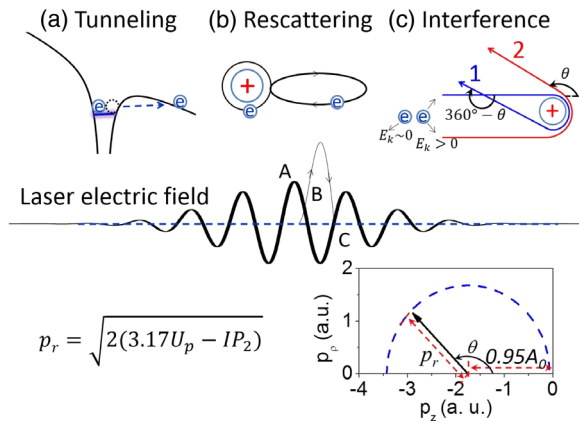


FIG. 1. Graphic illustration of extracting the DDCS from the momentum distribution of photoelectrons coincident with doubly charged ions. The strong-field rescattering process is depicted in the uppermost panel. In the top panel, A, B, and C illustrate the key steps of the ionization process, i.e., tunneling of the valence electron (A), which is accelerated and returns to the core (B). The tunneled electron may collide inelastically with the parent ionic core to induce double ionization, whereby two electrons are freed simultaneously. The kinetic energy of one electron is close to zero while that of the other one is significantly larger. The contributions of the two orbits of the higher-energy electron will interfere with each other (C); see the text for details. In the middle panel, the times of the events A, B, and C are marked on the temporal graph of the laser electric field. The black curve indicates the orbit with the highest return energy of $3.17 U_p$ for the recolliding electron. The lowermost panel shows the curve (the blue-dashed semicircle) along which the DDCS is extracted; see the text for details.

electron, as measured by the detector, corresponding to the recollision near the crest of the vector potential of the laser field and a maximal energy of $3.17U_p$ of the recolliding electron, can be calculated with $p_r = \sqrt{2(3.17U_p - IP_2)}$, where $U_p = A_0^2/4$ [A_0 denotes the maximum of $A(t)$] is the ponderomotive energy and IP_2 is the second ionization potential of the atomic target in question. Hence, the final-electron momentum lies on a circle in the (p_z, p_r) plane with a radius of p_r and its center at $(\pm A(t_r), 0)$, where $A(t_r) \approx 0.95A_0$, as shown in the lowermost panel of Fig. 1. To extract the DDCS for one electron released with near zero energy in the laser-induced (e , $2e$) process, we thus plot, as a function of the angle θ between the directions of the electron momentum before and after the scattering process in the frame of the ion, the yields of electron events on the circle.

The experiments have been performed with cold-target recoil-ion momentum spectroscopy (COLTRIMS) [16,17]. The femtosecond laser pulses employed in our experiments are generated from a commercial Ti:sapphire femtosecond laser system (FEMTOPOWER compact PRO CE-Phase HP/HR) with a repetition rate of 5 kHz, a pulse duration of around 30 fs, and a center wavelength of 800 nm. The laser beam is focused into the cold supersonic beam inside the COLTRIMS vacuum chamber, and the three-dimensional momenta of the photoelectrons and the doubly charged photoion are measured in coincidence. Before the laser beam is directed into the COLTRIMS apparatus, the laser-pulse energy is precisely controlled with a combination of a broadband achromatic $\lambda/2$ plate and a broadband thin-film polarizer. The laser intensities are calibrated with a procedure utilizing the photoelectron (photoion) momentum distribution in a close-to-circularly-polarized laser field with nonadiabatic effects included [18]. During the measurement, great attention is paid to keep the production rate of photoelectrons below 20% of the laser-pulse repetition rate, which ensures that less than one ionization event occurs for each pulse. The false coincidence ratio from the background is estimated to be around 6%.

Figure 2 shows typical 2D photoelectron momentum distributions measured in coincidence with doubly charged ions from NSDI of Xe and Ar at several laser intensities. One finds that the size of the photoelectron velocity map expands as the laser intensity (corresponding to A_0) increases, as expected. The circles employed to extract the DDCSs are indicated by black solid lines; their center positions and radii depend strongly on the atomic species and laser intensity, as determined by the LIID principle discussed above. The extracted DDCSs are depicted in Fig. 3. To avoid the disturbance from electrons that return with energies much lower than $3.17U_p$ from the NSDI process, the lower limit of the angular range is chosen to be 100° . It is also worth mentioning that the DDCSs can only be reliably extracted if there is no contamination from electrons generated by sequential double ionization (SDI).

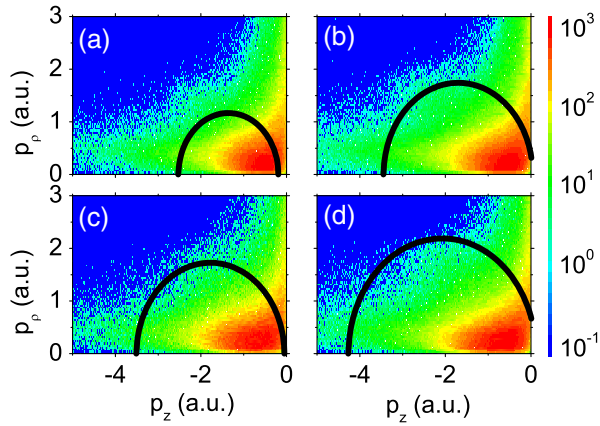


FIG. 2. The measured 2D photoelectron momentum distributions coincident with Xe^{2+} [(a) and (b)] and Ar^{2+} [(c) and (d)]. The laser intensities are (a) 2.0×10^{14} W/cm², (b) 3.3×10^{14} W/cm², (c) 3.6×10^{14} W/cm², and (d) 4.9×10^{14} W/cm². The black solid circle in each panel indicates the path employed to extract the DDCS.

Ideally, this would require that NSDI be dominant over SDI, as is the case for sufficiently low intensity [19–21]. Moreover, even if there is substantial SDI, one can still extract the DDCS for sufficiently high electron energy. Namely, electrons from SDI obey approximately the $2U_p$ cutoff of direct ionization, while electrons from the NSDI channel exhibit a much higher cutoff energy of about $6 - 7U_p$ [22–25]. Therefore, the influence of the SDI channel in the extracted DDCSs can be safely neglected in our case.

The DDCSs in Fig. 3 show a smooth evolution with increasing angle, with a prominent maximum around 180°

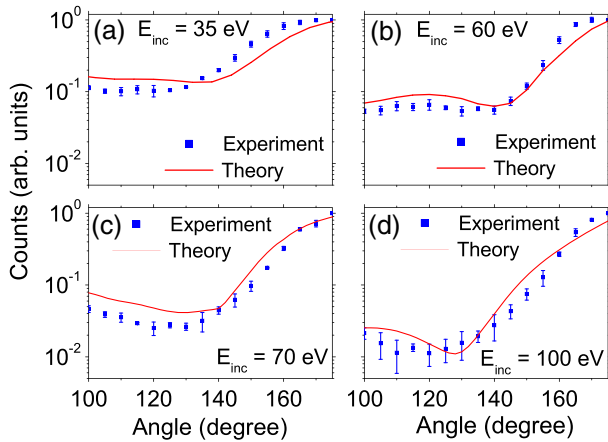


FIG. 3. Typical DDCSs extracted from the experimental data of Fig. 2 and the calculated DDCSs of Xe^+ [(a) and (b)] and Ar^+ [(c) and (d)] with incident electron energies of (a) 35 eV, (b) 60 eV, (c) 70 eV, and (d) 100 eV. The experimental (theoretical) data are indicated with blue filled squares (red solid curves). The laser intensities are identical to the ones in the corresponding panels of Fig. 2.

for every case, and the higher the laser intensity is, the steeper the curve evolves with the angle. In addition, each curve displays a minimum at some angle larger than 100° , which shifts with the laser intensity. On closer inspection, Fig. 3(b) shows an additional maximum at about 120° for Xe at 3.3×10^{14} W/cm². These structures are very similar to the angle-dependent ($e, 2e$) cross sections measured in conventional electron-impact ionization for various species of atoms and molecules [26].

For comparison, we used the distorted-wave Born approximation (DWBA) to calculate the DDCSs of Ar^+ and Xe^+ for different incident electron energies, each corresponding to the maximal return energy of the recolliding electron, i.e., $3.17U_p$, in the intense-field NSDI experiment. The DWBA treats the system as two electrons—namely, the incident electron and another one that is initially bound and then ionized—which interact with an inert core via potentials v_1 and v_2 and with one other via v_3 . In this treatment, the Hamiltonian of the system is partitioned as follows:

$$H = [(k_1 + v_1) + (k_2 + v_2)] + v_3 = H_0 + v_3, \quad (2)$$

where v_3 is the interaction between the two electrons and is treated as a scattering potential in this model. The wave functions of the continuum electrons can be obtained independently by solving the single-particle Schrödinger equation. The key point in the DWBA calculation is to choose distorting potentials U_1 and U_2 , which are local and central and as close as possible to v_1 and v_2 , respectively. In the calculation, the distorting potentials include two parts: a Slater-type direct distorting potential V_D [27] and a global semiclassical polarization potential V_{pol} [28]. Moreover, a modified semiclassical exchange (MSCE) potential V_E [29] was used to describe the exchange interaction, so that

$$v_i \approx U_i = V_D + V_{\text{pol}} + V_{E_i}, \quad (i = 1, 2) \quad (3)$$

where E_i denotes the energy of electron i .

Finally, the first-order T -matrix element of the DWBA can be written as

$$T_{fi} = \langle \chi^-(k_s) \chi^-(k_f) | v_3 | \alpha \chi^+(k_0) \rangle, \quad (4)$$

which can be solved using the partial-wave expansion method. The states $|\alpha \chi^+(k_0)\rangle$ and $|\chi^-(k_s) \chi^-(k_f)\rangle$ are the initial and final channel states, respectively, obtained from the product of single-particle wave functions. The triply and doubly differential cross sections of the scattered electrons can be obtained subsequently.

In the calculation, the kinetic energy of the slow ejected electron (E_s) is set to be 1 eV. It is worth noting that the calculated DDCS is hardly dependent on E_s provided it is

less than 1 eV. The calculated results are presented with red solid curves in Fig. 3 and show a rather good agreement with the experimental results. Each DDCS shows a maximum at 180° , and the maximum becomes more pronounced for higher incident electron energy. In addition, each DDCS exhibits a minimum between 120° and 140° . Moreover, a maximum around 120° for Xe^+ with an incident electron energy of 60 eV [see the red solid curve in Fig. 3(b)] is visible and qualitatively consistent with the experimental data.

The mechanism underlying the peculiar structure of the DDCS can be understood with the generalized Ramsauer-Townsend diffraction mechanism [30]. Namely, for a potential that increases faster than $1/r$ for $r \rightarrow 0$, the electron can loop around the target as shown in Fig. 1(c), and there are two different orbits which scatter into the same direction with different impact parameters and interfere with each other. For exact backscattering, i.e., $\theta = 180^\circ$, the two trajectories have the same phase and constructive interference occurs, resulting in a maximum at 180° in the DDCS. When the scattering angle decreases, the phase difference between the two trajectories increases, and therefore the DDCS decreases until it reaches a minimum when the interference becomes destructive. Since, as mentioned above, the electron can loop around only for potentials decreasing faster than $1/r$, the effect is more pronounced for heavier ions with more electrons screening the nucleus. Apparently, the rate of change of the phase difference strongly depends on the momentum of the ejected electron. The higher the momentum, the faster the phase difference changes [30]. Therefore, the DDCS decreases faster with decreasing angle and the minimum appears at a larger angle, in agreement with the experimental and theoretical results of Xe shown in Figs. 3(a) and 3(b). On the other hand, the detailed behavior of the cross section curve, e.g., the position of its minimum, is also dependent on the wave function of the bound electron, which leads to the fact that, for Ar, the DDCS curve for a lower incident electron energy exhibits a minimum at a larger angle than that for a higher incident energy, as shown in Figs. 3(c) and 3(d).

Careful inspection reveals some discrepancies between the experimental results and the DWBA calculations (see Fig. 3). For example, the positions of the minima are located at smaller angles in the experimental data than in the DWBA simulations. This quantitative discrepancy may be understood by the fact that the theoretical approach employed is essentially a one-particle model, which works well for high-energy collisions [27]. However, in the present case, since the incident electron energies are not high enough (less than 100 eV) and the ejected electron energy is very low ($= 1$ eV), it is thus expected that the electron-correlation effects become important and need to be considered explicitly. In addition, for the present DWBA treatment, in spite of the fact that an advanced MSCE exchange potential and a global polarization potential have

been employed to model the complex short-range interaction, the contribution of excited-state channels is still neglected, which has been proven to be important in low-energy (e , $2e$) reactions [31]. In order to achieve better agreement with the measurements, more realistic models are required, such as convergent close-coupling [32] and B -spline R -matrix [31] methods, etc.

To summarize, a novel laser-induced inelastic-diffraction (LIID) approach, based on the atomic nonsequential-double-ionization process driven by an intense femtosecond laser field, has been proposed. In this NSDI process, the double electron emission is caused by an (e , $2e$) process triggered by the tunneled electron and the electron-electron correlation, which plays a paramount role. We apply this approach, for the first time, to extract the DDCSs of singly charged ions of noble gases in the (e , $2e$) process from the 2D photoelectron momentum distributions in nonsequential double ionization. The extracted DDCSs are well consistent with theoretical calculations based on the distorted-wave Born approximation. The peculiar angular structure in the extracted DDCS can be understood by considering the generalized Ramsauer-Townsend diffraction effect and the wave function of the ion.

Looking forward, we expect that this LIID approach, when applied to gas-phase molecular systems, can be used to image the ultrafast evolution of the molecular structure and dynamics induced by the strong laser field, similarly to the well-established LIED scheme [13,14]. More specifically, in the LIID scheme, the inelastic collision time can be finely tuned by changing the laser wavelength, since the propagation time of the incident (i.e., the tunneled) electron is proportional to the oscillation period of the laser field. During a molecular reaction, the dynamical electron correlation effect, which is dependent on the molecular nuclear distances, can thus be deduced from the DDCSs extracted at different laser wavelengths. Compared with LIED, this LIID approach is expected to shed more light on the complex molecular dynamics induced by a strong laser field, especially for those processes where the dynamical electron correlation is important, e.g., the dissociative ionization process of molecules which is triggered by the laser-induced (e , $2e$) process, with unprecedented attosecond temporal resolution.

We are grateful to Professor X. W. Ma for many useful discussions. This work is supported by the National Key Research and Development Program of China (No. 2016YFA0401100 and No. 2017YFA0402300), the National Basic Research Program of China (No. 2013CB922200), the National Natural Science Foundation of China (No. 11334009, No. 11374329, No. 11425414, No. 11474321, No. 11534011, and No. U1530261), and the Strategic Priority Research Program of the Chinese Academy of Sciences (No. XDB21010400).

- *wu_yong@iapcm.ac.cn
 †xjliu@wipm.ac.cn
 ‡chen_jing@wipm.ac.cn
- [1] M. P. Miniti, J. M. Budarz, A. Kirrander, J. S. Robinson, D. Ratner, T. J. Lane, D. Zhu, J. M. Glowina, M. Kozina, H. T. Lemke, M. Sikorski, Y. Feng, S. Nelson, K. Saita, B. Stankus, T. Northey, J. B. Hastings, and P. M. Weber, Imaging molecular motion: Femtosecond X-Ray Scattering of an Electrocyclic Chemical Reaction, *Phys. Rev. Lett.* **114**, 255501 (2015).
- [2] A. H. Zewail, Femtochemistry: Atomic-scale dynamics of the chemical bond using ultrafast lasers, *Angew. Chem., Int. Ed. Engl.* **39**, 2587 (2000).
- [3] P. Reckenthaeler, M. Centurion, W. Fuß, S. A. Trushin, F. Krausz, and E. E. Fill, Time-Resolved Electron Diffraction from Selectively Aligned Molecules, *Phys. Rev. Lett.* **102**, 213001 (2009).
- [4] C. Gerbig, A. Senftleben, S. Morgenstern, C. Sarpe, and T. Baumert, Spatio-temporal resolution studies on a highly compact ultrafast electron diffractometer, *New J. Phys.* **17**, 043050 (2015).
- [5] P. B. Corkum, Plasma Perspective on Strong-Field Multiphoton Ionization, *Phys. Rev. Lett.* **71**, 1994 (1993).
- [6] K. J. Schafer, B. Yang, L. F. DiMauro, and K. C. Kulander, Above Threshold Ionization beyond the High Harmonic Cutoff, *Phys. Rev. Lett.* **70**, 1599 (1993).
- [7] S. Baker, J. S. Robinson, C. A. Haworth, H. Teng, R. A. Smith, C. C. Chirilă, M. Lein, J. W. G. Tisch, and J. P. Marangos, Probing proton dynamics in molecules on an attosecond time scale, *Science* **312**, 424 (2006).
- [8] R. Torres, T. Siegel, L. Brugnera, I. Procino, J. G. Underwood, C. Altucci, R. Velotta, E. Springate, C. Froud, I. C. E. Turcu, S. Patchkovskii, M. Yu. Ivanov, O. Smirnova, and J. P. Marangos, Revealing molecular structure and dynamics through high-order harmonic generation driven by mid-IR fields, *Phys. Rev. A* **81**, 051802(R) (2010).
- [9] T. Morishita, A.-T. Le, Z. Chen, and C. D. Lin, Accurate Retrieval of Structural Information from Laser-Induced Photoelectron and High-Order Harmonic Spectra by Few-Cycle Laser Pulses, *Phys. Rev. Lett.* **100**, 013903 (2008).
- [10] M. Okunishi, T. Morishita, G. Prümper, K. Shimada, C. D. Lin, S. Watanabe, and K. Ueda, Experimental Retrieval of Target Structure Information from Laser-Induced Rescattered Photoelectron Momentum Distributions, *Phys. Rev. Lett.* **100**, 143001 (2008).
- [11] D. Ray, B. Ulrich, I. Bocharova, C. Maharjan, P. Ranitovic, B. Gramkow, M. Magrakvelidze, S. De, I. V. Litvinyuk, A. T. Le, T. Morishita, C. D. Lin, G. G. Paulus, and C. L. Cocke, Large-Angle Electron Diffraction Structure in Laser-Induced Rescattering from Rare Gases, *Phys. Rev. Lett.* **100**, 143002 (2008).
- [12] M. Meckel, D. Comtois, D. Zeidler, A. Staudte, D. Pavičić, H. C. Bandulet, H. Pépin, J. C. Kieffer, R. Dörner, D. M. Villeneuve, and P. B. Corkum, Laser-induced electron tunneling and diffraction, *Science* **320**, 1478 (2008).
- [13] C. I. Blaga, J. Xu, A. D. DiChiara, E. Sistrunk, K. Zhang, P. Agostini, T. A. Miller, L. F. DiMauro, and C. D. Lin, Imaging ultrafast molecular dynamics with laser-induced electron diffraction, *Nature (London)* **483**, 194 (2012).
- [14] B. Wolter, M. G. Pullen, A.-T. Le, M. Baudisch, K. Doblhoff-Dier, A. Senftleben, M. Hemmer, C. D. Schröter, J. Ullrich, T. Pfeifer, R. Moshhammer, S. Gräfe, O. Vendrell, C. D. Lin, and J. Biegert, Ultrafast electron diffraction imaging of bond breaking in di-ionized acetylene, *Science* **354**, 308 (2016).
- [15] For recent reviews on NSDI, see, e.g., A. Becker, R. Dörner, and R. Moshhammer, Multiple fragmentation of atoms in femtosecond laser pulses, *J. Phys. B* **38**, S753 (2005); C. F. de Morisson Faria and X. Liu, Electron-electron correlation in strong laser fields, *J. Mod. Opt.* **58**, 1076 (2011); W. Becker, X. Liu, P. J. Ho, and J. H. Eberly, Theories of photoelectron correlation in laser-driven multiple atomic ionization, *Rev. Mod. Phys.* **84**, 1011 (2012).
- [16] J. Ullrich, R. Moshhammer, A. Dorn, R. Dörner, L. Ph. H. Schmidt, and H. Schmidt-Böcking, Recoil-ion and electron momentum spectroscopy: Reaction-microscopes, *Rep. Prog. Phys.* **66**, 1463 (2003).
- [17] Y. Wang, S. Xu, W. Quan, C. Gong, X. Lai, S. Hu, M. Liu, J. Chen, and X. Liu, Recoil-ion momentum distribution for nonsequential double ionization of Xe in intense midinfrared laser fields, *Phys. Rev. A* **94**, 053412 (2016).
- [18] W. Quan, M. Yuan, S. Yu, S. Xu, Y. Chen, Y. Wang, R. Sun, Z. Xiao, C. Gong, L. Hua, X. Lai, X. Liu, and J. Chen, Laser intensity determination using nonadiabatic tunneling ionization of atoms in close-to-circularly polarized laser fields, *Opt. Express* **24**, 23248 (2016).
- [19] S. Laroche, A. Talebpour, and S. L. Chin, Non-sequential multiple ionization of rare gas atoms in a Ti:sapphire laser field, *J. Phys. B* **31**, 1201 (1998).
- [20] J. L. Chaloupka, R. Lafon, L. F. DiMauro, P. Agostini, and K. C. Kulander, Observation of a Transition in the Dynamics of Strong-Field Double Ionization, *Phys. Rev. Lett.* **90**, 033002 (2003).
- [21] Note that the femtosecond laser pulse duration employed in our work is much shorter than those in Refs. [19] and [20], which will increase significantly the saturation intensity of single ionization for noble gas atoms and favor the channel of nonsequential double ionization over the sequential one.
- [22] J. L. Chaloupka, R. Lafon, L. F. DiMauro, P. Agostini, and K. C. Kulander, Strong-field double ionization of rare gases, *Opt. Express* **8**, 352 (2001).
- [23] J. Chen, J. Liu, and W. M. Zheng, Characteristic photoelectron spectra and angular distributions of single and double ionization, *Phys. Rev. A* **66**, 043410 (2002).
- [24] D. B. Milošević and W. Becker, Classical cutoffs for laser-induced nonsequential double ionization, *Phys. Rev. A* **68**, 065401 (2003).
- [25] J. S. Parker, B. J. S. Doherty, K. T. Taylor, K. D. Schultz, C. I. Blaga, and L. F. DiMauro, High-Energy Cutoff in the Spectrum of Strong-Field Nonsequential Double Ionization, *Phys. Rev. Lett.* **96**, 133001 (2006).
- [26] S. Yan, X. Ma, P. Zhang, S. Xu, S. F. Zhang, X. L. Zhu, W. T. Feng, and H. P. Liu, Evidence of strong projectile-target-core interaction in single ionization of neon by electron impact, *Phys. Rev. A* **82**, 052702 (2010).
- [27] I. E. McCarthy, Distorted-wave Born and impulse approximations for electron-atom ionization, *Aust. J. Phys.* **48**, 1 (1995); X. Hu, C.-Z. Gao, Z. Chen, J. Wang, Y. Wu, and Y. Wang, Electron-impact ionization of Ne(2p) and Ar(3p) at

- intermediate energies: Role of the postcollision interaction, *Phys. Rev. A* **96**, 052701 (2017).
- [28] F. A. Gianturco, K. T. Tang, J. P. Toennies, D. De Fazio, and J. A. Rodriguez-Ruiz, A semiclassical model of polarization forces in atomic scattering: II. Electron collisions with neon and argon, *Z. Phys. D* **33**, 27 (1995).
- [29] F. A. Gianturco and S. Scialla, Local approximations of exchange interaction in electron-molecule collisions: The methane molecule, *J. Phys. B* **20**, 3171 (1987).
- [30] W. F. Egelhoff, Jr., Semiclassical Explanation of the Generalized Ramsauer-Townsend Minima in Electron-Atom Scattering, *Phys. Rev. Lett.* **71**, 2883 (1993).
- [31] O. Zatsarinny and K. Bartschat, Nonperturbative Treatment of Ionization with Excitation of Helium by Electron Impact, *Phys. Rev. Lett.* **107**, 023203 (2011).
- [32] I. Bray, D. V. Fursa, A. S. Kadyrov, A. T. Stelbovics, A. S. Kheifets, and A. M. Mukhamedzhanov, Electron- and photon-impact atomic ionisation, *Phys. Rep.* **520**, 135 (2012).